Synthesis and Characterization of Ag−Hollandite Nanofibers and Its Catalytic Application in Ethanol Oxidation

Junli Chen, Xingfu Tang, Junlong Liu, Ensheng Zhan, Juan Li, Xiumin Huang, and Wenjie Shen*

State Key Laboratory of Catalysis, Dalian Institute of Chemical Physics, Chinese Academy of Sciences, Dalian 116023, China

Received April 1, 2007. Revised Manuscript Received June 18, 2007

Ag−hollandite nanofibers were synthesized through a simple hydrothermal process by oxidizing $Mn(NO_3)_2$ with $AgMnO_4$ in aqueous solution. The temperature was found to play an essential role in determining both the crystalline structure and the morphology of the Ag−hollandite materials, whereas the $AgMnO_4/Mn(NO_3)_2$ molar ratio affected only the morphology of the product. Ag−hollandite nanofibers with diameters of 20−40 nm and lengths of 0.5−4 μm were prepared at 160 °C and a 2/3 $AgMnO_4/Mn(NO_3)_2$ molar ratio. X-ray photoelectron spectroscopy surface analysis revealed that the silver species presented as Ag^+ and the average oxidation state of manganese was 3.9. More promisingly, the Ag−hollandite nanofibers showed quite high catalytic performance for ethanol oxidation, with ethanol conversion of 75% and acetaldehyde selectivity of 95% at 230 °C for 200 h time-on-stream. The high activity, selectivity, and stability were attributed to the stable presence of Ag^+ species and the unique morphology of the Ag−hollandite nanofibers.

Introduction

Hollandite-type manganese oxide materials, also known as octahedral molecular sieves (OMS-2), consist of a one-dimensional tunnel (0.46 nm × 0.46 nm) structure surrounded by interlinking of edge-shared MnO_6 octahedral units. Manganese in the octahedra is mainly presented as Mn^{4+} and Mn^{3+}, and cations such as K^+, Ba^{2+}, and/or a small amount of H_2O molecule partially occupy the tunnel to provide charge balance and stabilize the tunnel structure.[1] Because of the unique microporous feature and the mixed manganese valencies, hollandite-type manganese oxides have been extensively studied for potential applications as ion or molecular sieves,[2] oxidation catalysts,[3] and rechargeable battery materials.[4] For further improving the electronic and catalytic properties of the traditional hollandite-type manganese oxides (K−OMS-2), other metal cations were introduced into the tunnel by post ion exchange[2b,5] or into the framework by substitution during synthesis.[6] Isomorphous substitution of manganese ions in the framework with cations like Fe^{3+} and V^{5+} was recently reported by Suib and coworkers.[7] They found that the doping of vanadium into the framework of the hollandite structure could lower the average oxidation state of manganese and increase the electrical resistivity.[7b]

The introduction of alkali and/or transition metal cations into the tunnel could also significantly modify the physical and chemical properties of hollandite-type manganese oxides. Liu et al.[8] synthesized hollandite-type manganese oxides with Li^+, Na^+, K^+, Rb^+, and NH^{4+} as tunnel cations and found that the nature of the cation greatly affected the properties of the OMS-2 materials, such as crystallinity, microstructure, thermal stability, and catalytic activity for aerobic oxidation of cyclohexanol. Meanwhile, transition metal cations in the tunnels were also observed to greatly promote the catalytic properties of the OMS-2 materials.[5−6] Octahedral molecular sieves with Co^{2+}, Ag^+, and Cu^{2+} as tunnel cations showed high catalytic activities for CO oxidation at low temperatures.[5] The charge transfer along the M−O−Mn bond (M = Co, Ag, Cu) was suggested to be responsible for the high catalytic properties. For example, the Ag^+ cation in Ag−OMS-2 may abstract electrons from oxygen anions through the Ag−O−Mn bridge, near which the oxygen molecule was

* Corresponding author. Tel: 86-411-84379085. Fax: 86-411-84694447. E-mail: shen98@dicp.ac.cn.

(1) (a) Shen, Y. F.; Serger, R. P.; Deguzman, R. N.; Suib, S. L.; Mccurdy, L.; Potter, D. I.; O'Young, C. L. *Science* **1993**, *260*, 511−515. (b) Giraldo, O.; Brock, S. L.; Marquez, M.; Suib, S. L.; Hillhouse, H.; Tsapatsis, M. *Nature* **2000**, *405*, 38. (c) Feng, Q.; Kanoh, H.; Ooi, K. *J. Mater. Chem.* **1999**, *9*, 319−333.

(2) (a) Feng, Q.; Kanoh, H.; Miyai, Y.; Ooi, K. *Chem. Mater.* **1995**, *7*, 148−153. (b) Dyer, A.; Pillinger, M.; Newton, J.; Harjula, R.; Möller, T.; Amin, S. *Chem. Mater.* **2000**, *12*, 3798−3804.

(3) (a) Son, Y. C.; Makwana, V. D.; Howell, A. R.; Suib, S. L. *Angew. Chem., Int. Ed.* **2001**, *40*, 4280−4283. (b) Ghosh, R.; Shen, X. F.; Villegas, J. C.; Ding, Y. S.; Malinger, K.; Suib, S. L. *J. Phys. Chem. B* **2006**, *110*, 7592−7599. (c) Ghosh, R.; Son, Y. C.; Makwana, V. D.; Suib, S. L. *J. Catal.* **2004**, *224*, 288−296. (d) Vileno, E.; Zhou, H.; Zhang, Q.; Suib, S. L.; Corbin, D. R.; Koch, T. A. *J. Catal.* **1999**, *187*, 285−297.

(4) (a) Clearfield, A. *Chem. Rev.* **1988**, *88*, 125−148. (b) Dai, J. X.; Li, S. F. Y.; Siow, K. S.; Gao, Z. Q. *Electrochim. Acta* **2000**, *45*, 2211−2217. (c) Noailles, L. D.; Johnson, C. S.; Vaughey, J. T.; Thackeray, M. M. *J. Power Sources* 1999, 81−82, 259−263.

(5) Xia, G. G.; Yin, Y. G.; Willis, W. S.; Wang, J. Y.; Suib, S. L. *J. Catal.* **1999**, *185*, 91−105.

(6) (a) Chen, X.; Shen, Y. F.; Suib, S. L.; O'Young, C. L. *Chem. Mater.* **2002**, *14*, 940−948. (b) Chen, X.; Shen, Y. F.; Suib, S. L.; O'Young, C. L. *J. Catal.* **2001**, *197*, 292−302.

(7) (a) Cai, J.; Liu, J.; Willis, W. S.; Suib, S. L. *Chem. Mater.* **2001**, *13*, 2413−2422. (b) Polverejan, M.; Villegas, J. C.; Suib, S. L. *J. Am. Chem. Soc.* **2004**, *126*, 7774−7775.

(8) Liu, J.; Makwana, V.; Cai, J.; Shen, X. F.; Suib, S. L.; Aindow, M. *J. Phys. Chem. B* **2003**, *107*, 9185−9194.

10.1021/cm070904k CCC: $37.00
Published on Web 07/27/2007

possibly chemisorbed. However, the introduction of the Ag^+ cation into the tunnel also made the typical hollandite crystal structure in Ag−OMS-2 disappear, and the crystallinity became very poor.[6]

For the first time, Chang and Jansen[9] synthesized Ag−hollandite materials by solid-state reaction of $AgMnO_4$ and Ag_2O at 970 °C and a very high oxygen pressure for 7 days. Compared with the K−OMS-2 materials, the structure of Ag−hollandite was slightly modified in which the silver cation did not occupy the centers of the cubic cages formed by MnO_6 octahedra, but located on the common faces of the cubes. The needlelike crystal was very large with dimensions of $0.1 \times 0.4 \times 1.0$ mm^3, resulting in very low available surface area. Most recently, Li and King[10] synthesized Ag−hollandite by ion exchange of K−OMS-2 in melt $AgNO_3$, and the obtained materials had much smaller needlelike crystals (about 30 nm width and 100−200 nm long) and relatively high surface area (35 m^2/g). More importantly, this Ag−hollandite could act as an excellent low-temperature (150 °C) SO_2 absorbent and a highly active catalyst for CO and NO oxidation. However, there were still K^+ cations remaining in the tunnel and significant amounts of metallic Ag particles were present in the preface of the Ag−hollandite. Because metallic silver is a well-known oxidation catalyst,[11] it is difficult to attribute the high catalytic activities for CO and NO oxidation exclusively to the Ag−hollandite phase.

In this work, we report the synthesis of Ag−hollandite nanofibers by a hydrothermal process under very mild conditions. The effects of the temperature and the concentration of Ag^+ cation on the crystallography and morphology of Ag−hollandite materials were investigated. The formation mechanism of Ag−hollandite nanofibers was proposed through XRD and TEM studies. The catalytic performance of the Ag−hollandite nanofibers was tested for ethanol oxidation reaction.

Experimental Section

Synthesis. $AgMnO_4$ was synthesized by the reaction of $KMnO_4$ with $AgNO_3$ in aqueous solution. One hundred grams of $KMnO_4$ was dissolved into 2 L of boiling deionized water, and 50 mL of $AgNO_3$ aqueous solution (13 M) was then gradually added under stirring at 100 °C. The mixed solution was maintained at 100 °C for 30 min. After filtration, the precipitate was thoroughly washed with deionized water and dried at 60 °C for 4 h under a vacuum.

The Ag−hollandite was prepared by hydrothermal synthesis method. Typically, 0.4763 g of $AgMnO_4$ was dissolved into 40 mL of deionized water, to which 2 mL of concentrated HNO_3 solution was added to form a purple solution. $Mn(NO_3)_2$ (0.5637 g) dissolved in 40 mL of deionized water was then gradually added to the $AgMnO_4$ solution under vigorous stirring at room temperature. The mixture was sealed into a 100 mL Teflon-lined stainless steel autoclave, heated to a desired temperature (120−200 °C), and kept at this temperature for 12 h (unless noted elsewhere). After being cooled to room temperature, the obtained solid was filtered, washed thoroughly with deionized water, and dried at 100 °C overnight. **A**g−hollandites (0.47 g) were obtained after drying with a yield of about 97%. Ag−hollandites with different $AgMnO_4$/Mn-$(NO_3)_2$ molar ratios were also synthesized at 160 °C by the same procedure.

Characterization. *Structure Determination.* The X-ray powder diffraction (XRD) patterns of the samples were recorded with a D/Max-2500/PC powder diffractometer (Rigaku, Japan) operated at 40 kV and 100 mA, using nickel-filtered Cu Kα ($\lambda = 0.15418$ nm) radiation. The transmission electron microscope (TEM) images of the materials were obtained using a JEOL JEM-2000EX instrument with an acceleration voltage of at 120 kV. The samples were dispersed into ethanol with ultrasonic treatment for several minutes, and drops of the suspension were placed on a copper grid for TEM observations. This high-resolution transmission electron microscopy (HRTEM) images were recorded on a Philips Tecnai G^{2}20 operated at 300 kV. The morphologies of the Ag−hollandite materials were recorded using a Philips Fei Quanta 200F field-emission scanning electron microscope (FESEM). The powder sample was dispersed on a conductive adhesive tape.

Element Analysis. The elemental analysis of the samples was performed by inductively coupled plasma atomic emission spectroscopy (ICP-AES) on a Plasma-Spec-I spectrometer. About 20 mg of sample was dissolved into 10 mL of a 2% HNO_3/30% H_2O_2 aqueous solution, and the mixture was then diluted with 2% HNO_3 to meet the detection range of the instrument.

N_2 Adsorption−Desorption Isotherms. The N_2 adsorption−desorption isotherm was performed on a Micromeritics ASAP 2010 system at −196 °C. Prior to measurement, the samples were degassed at 300 °C for 8 h. The specific surface areas (S_{BET}) were calculated by a multipoint Braunauer−Emmett−Teller method, and the pore size distribution was determined by the H−K method.

Surface Analysis. X-ray photoelectron spectroscopy (XPS) was performed with an ESCALAB MK−II spectrometer (VG Scientific Ltd., UK) using Al Kα ($\lambda = 1486.6$ eV) radiation operated at an accelerating voltage of 12.5 kV. The powder samples were pressed into thin discs and mounted on a sample rod placed in an analysis chamber, where the spectra of Ag 3d, Ag MVV, Mn 2p, Mn 3s, and O 1s were recorded. Charging effects were corrected by adjusting the binding energy of C 1s to 284.6 eV.

Thermal Stability. The thermal stability of the materials was studied by thermogravimetric analyses (TGA) and temperature-programmed decomposition with mass spectroscopy. TGA was measured on a Pyris Diamond of Perkin-Elmer from room temperature to 900 °C under flowing helium. Thermal decomposition of the materials was performed in a fixed-bed quartz reactor and the temperature was programmed to rise at a ramp of 10 °C/min from room temperature to 900 °C using He as the carrier gas. The effluent species leaving the reactor were analyzed by an online mass spectrometer, and the *m*/*e* intensities at 18 (H_2O) and 32 (O_2) were recorded as a function of temperature.

Catalytic Evaluation. The oxidation of ethanol was conducted with a continuous-flow fixed-bed quartz reactor (6 mm in diameter and 35 cm in length) in the temperature range of 130−290 °C under atmospheric pressure. Fifty milligrams of catalyst (40−60 mesh) was diluted with 200 mg of quartz powder to prevent the temperature gradient in the catalyst bed and was charged into the reactor. Vapor ethanol was generated by flowing He over pure liquid ethanol in an incubator kept at 30 °C. The ethanol/He stream was then mixed with a stream of O_2/He coming from a mass flow controller, leading to a feed gas composition of 5.0% ethanol and 10% oxygen balanced by helium. The total flow rate was 30 mL/

(9) (a) Chang, F. M.; Jansen, M. *Angew. Chem., Int. Ed.* **1984**, *23*, 906−907. (b) Chang, F. M.; Jansen, M. *Rev. Chim. Mineral.* **1986**, *23*, 48−54.
(10) Li, L. Y.; King, D. L. *Chem. Mater.* **2005**, *17*, 4335−4343.
(11) (a) Qu, Z. P; Huang W. X; Zhou S. T; Zheng H.; Liu X. M; Cheng M. J.; Bao X. H. *J. Catal.* **2005**, *234*, 33−36. (b) Shen, J.; Shan, W.; Zhang, Y. H.; Du, J. M.; Xu, H. L.; Fan, K. N.; Shen, W.; Tang, Y. *J. Catal.* **2006**, *237*, 94−101.

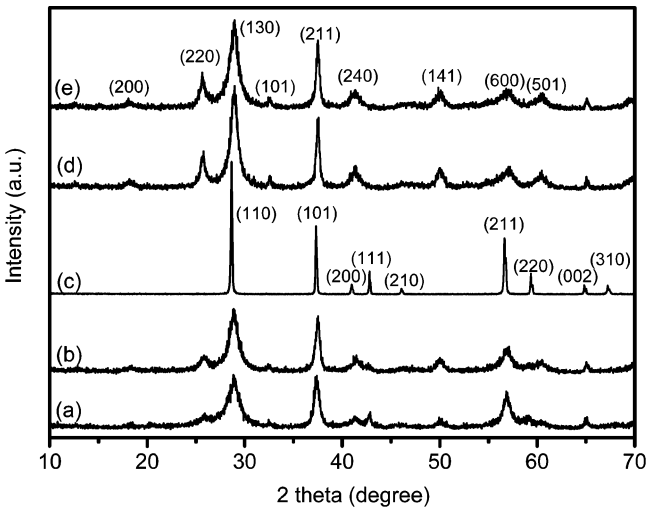

Figure 1. XRD patterns of the Ag−hollandite materials synthesized at (a) 120, (b) 160, and (c) 200 °C with a 2/3 $AgMnO_4/Mn(NO_3)_2$ ratio; Ag−hollandite materials synthesized at 160 °C with (d) 6/1 and (e) 5/2 $AgMnO_4/Mn(NO_3)_2$ molar ratios.

min, corresponding to a gas hourly space velocity of 36 000 mL g_{cat}^{-1} h^{-1}. The effluents from the reactor were analyzed by an on-line gas chromatograph (Varian 3800) equipped with TCD and FID detectors. A TDX-01 and Porapak Q combined packed column was used for the separation of regular gases and a PLOT Q capillary column connected to the FID detector was used for the separation of ethanol, acetaldehyde, acetic acid, and other organic products.

Results and Discussion

Crystal Structure and Morphology. Figure 1 shows the XRD patterns of the samples synthesized at 120−200 °C and $AgMnO_4/Mn(NO_3)_2$ molar ratios of 2/3 to 6/1. For the samples synthesized at 120−160 °C with a 2/3 $AgMnO_4/Mn(NO_3)_2$ ratio, the diffractions could be attributed to typical tetragonal crystal structure of Ag−hollandite (JCPDS 77-1987). There were no diffraction peaks due to silver species, indicating that the silver species were highly dispersed. The crystallinities were estimated to be 89% at 120 °C and 99% at 160 °C, and the corresponding crystalline sizes were 6 and 7 nm, respectively, calculated from the (130) diffraction lines. Hence, the temperature affected the crystal structure of the Ag−hollandites. The sharp and intensive diffraction peaks in the XRD pattern of the sample synthesized at 200 °C, however, indicated the crystal structure of pyrolusite (β-MnO_2, JCPDS 2-0735) and that the crystallite size calculated from the (110) diffraction line was more than 100 nm. Pyrolusite is thermodynamically more stable than hollandite-type manganese oxides, and thus a higher synthesis temperature usually favors the phase transformation from hollandite to pyrolusite.[12] On the other hand, relatively higher hydrothermal temperature is necessary to achieve better crystallinity of Ag−hollandite, as confirmed by the XRD profiles. Therefore, the temperature of 160 °C appears to be appropriate for the synthesis of Ag−hollandite materials with crystallinity of 99%.

Figure 1 also illustrates the XRD patterns of the materials synthesized at 160 °C with $AgMnO_4/Mn(NO_3)_2$ molar ratios of 2/3 to 6/1. Clearly, the characteristic reflections could be indexed to the tetragonal phase of Ag−hollandite, regardless of the $AgMnO_4/Mn(NO_3)_2$ molar ratio. Meanwhile, the crystallite size increased only marginally, from 7 to 10 nm, when the $AgMnO_4/Mn(NO_3)_2$ molar ratio was increased from 2/3 to 6/1, implying that the Ag^+ concentration in the range of 0.025−0.056 mol/L had almost no influence on the crystal structure of the Ag−hollandites. This phenomenon is somewhat different from previous observations for the K−OMS-2 materials. Wang and Li[13] found that the K^+ concentration could significantly affect the crystal structure of OMS-2 materials by reacting $KMnO_4$ with $MnSO_4$ and adjusting the molar ratio of $KMnO_4/MnSO_4$ between 5/2 and 2/3. Vernadite was produced at higher K^+ concentration, whereas hollandite and pyrolusite were obtained at relatively lower K^+ concentration. The discrepancy between Ag^+ and K^+ is probably caused by the template-directing effect of the two cations in the tunnel. According to Dyer et al.,[2b] hollandite is very effective for selective adsorption of Ag^+ in strong acidic solution, even in the presence of large amounts of other cations such as K^+, Cs^+, and Sr^{2+}. Hence, the temperature plays an essential role in determining the crystal structure of the silver hollandite-type manganese oxides, and the concentration of Ag^+ almost does not affect the crystal structure.

Figure 2 shows the FESEM and TEM images of the materials synthesized at different temperature and $AgMnO_4/Mn(NO_3)_2$ molar ratios. For the materials prepared using the identical $AgMnO_4/Mn(NO_3)_2$ ratio of 2/3, hydrothermal synthesis at 120 °C produced nanofibrous shapes with diameters of 10−40 nm and lengths of several micrometers. Simultaneously, significant amounts (up to about 30%) of nanoparticles with sizes of 100−200 nm were also produced. When the temperature was increased to 160 °C, very uniform nanofibers was obtained with diameters of 20−40 nm and lengths of 0.5−4.0 μm. Differently, the pyrolusite synthesized at 200 °C consisted of very larger polyhedron shapes with sizes of 0.2−2.5 μm. For the samples synthesized at 160 °C with different $AgMnO_4/Mn(NO_3)_2$ molar ratios, the concentration of Ag^+ remarkably affected the dimensions of the nanofibers. When the $AgMnO_4/Mn(NO_3)_2$ ratio was increased from 2/3 to 5/2, the diameter of the Ag−hollandite nanofibers rapidly increased to about 150 nm and the length significantly increased to several micrometers. Therefore, it is clear that both the temperature and the concentration of Ag^+ affected the morphologies of the Ag−hollandite materials.

Texture Properties. Table 1 summarizes the texture properties of the Ag−hollandite nanofibers synthesized at 160 °C. The Ag/Mn atomic ratio in the nanofibers increased from 0.087 to 0.111 when the $AgMnO_4/Mn(NO_3)_2$ molar ratio was increased from 2/3 to 5/2 in the reactant solution. These values are relatively less than the previously reported ones for Ag−hollandite materials (0.225[9] and 0.140[10]). This phenomenon indicates that there existed relatively more hydronium ion in the tunnel as a stabilizing counterion, in addition to Ag^+. The BET surface area (S_{BET}) of the Ag−

(12) Walanda, D. K.; Laurance, G. A.; Donne, S. W. *J. Power Sources* **2005**, *139*, 325−341.

(13) Wang, X.; Li, Y. D. *Chem.−Eur. J.* **2003**, *9*, 300−306.

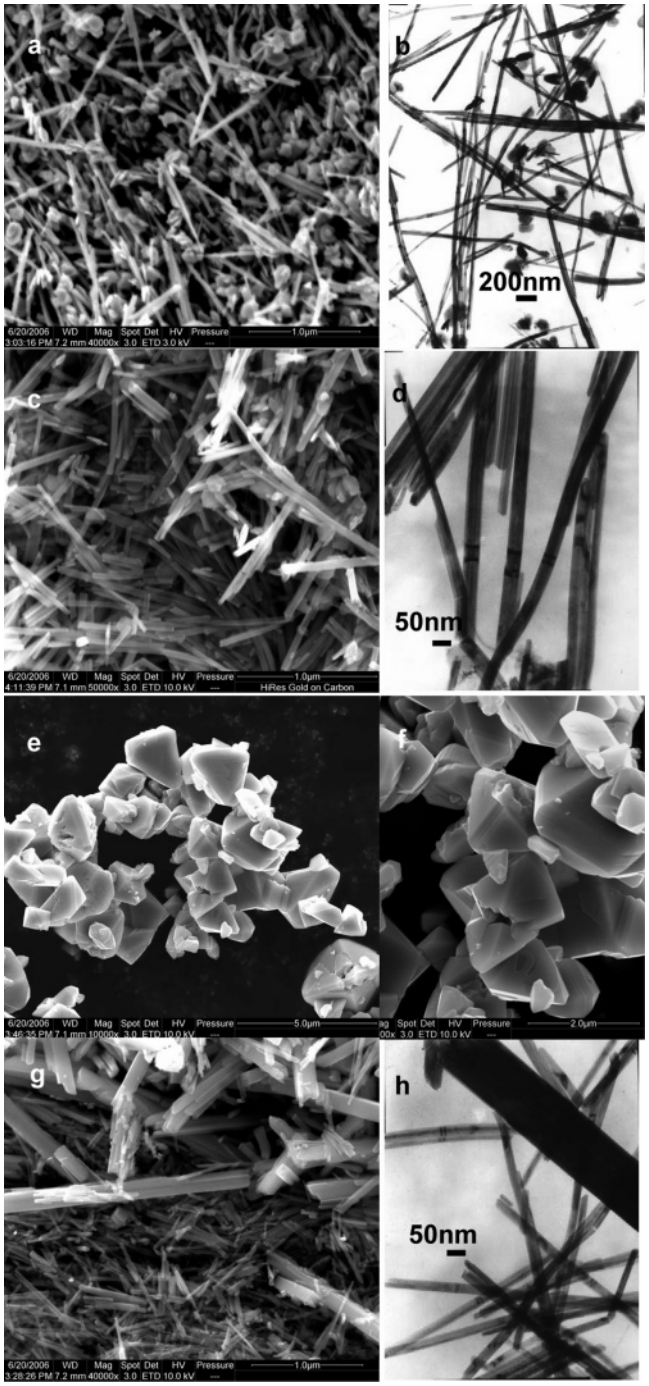

Figure 2. FESEM and TEM images of the materials synthesized at (a, b) 120, (c, d) 160, and (e, f) 200 °C with a 2/3 $AgMnO_4/Mn(NO_3)_2$ molar ratio, and (g, h) at 160 °C with a 5/2 $AgMnO_4/Mn(NO_3)_2$ molar ratio.

hollandite nanofibers only slightly increased from 42 to 46 m^2/g. Moreover, the external surface areas were very close to the total surface areas, indicating that the S_{BET} was mainly contributed to by the external surface. Similarly, the micropore volume contributed to only less than 7% of the total pore volume. This can be understood by considering the unique microporous structure of OMS-2 materials. Although the hollandite manganese oxides have a crystalline pore opening of about 0.46 nm, the effective pore opening may be in a range of about 0.265−0.333 nm according to the adsorption isotherms with different adsorbates.[14] Thus, only a small fraction of nitrogen with a dynamic diameter of 0.364 nm could enter into the tunnels of Ag−hollandite nanofibers,

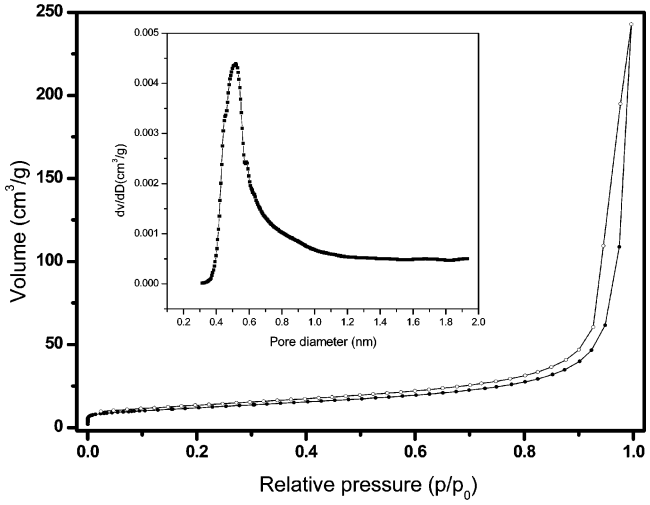

Figure 3. N_2 adsorption−desorption isotherm and pore-size distribution of the Ag−hollandite nanofibers.

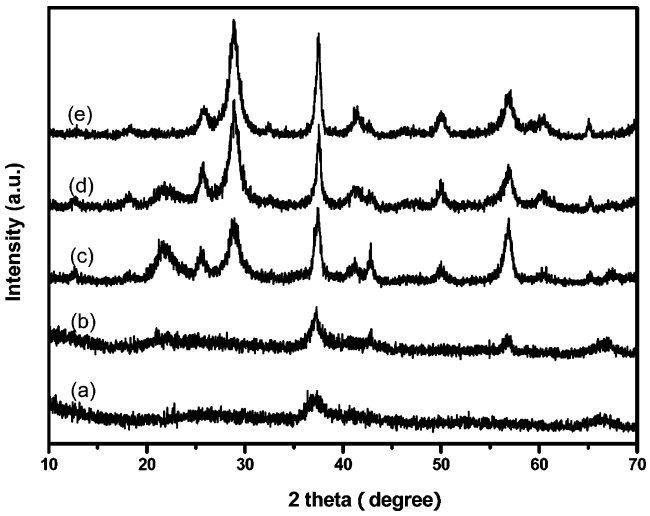

Figure 4. XRD patterns of the samples at different stages of hydrothermal synthesis: (a) precursor at room temperature, and at 160 °C for (b) 0.5, (c) 1, (d) 6, and (e) 12 h.

resulting in lower than estimated contribution of the micropores.

Figure 3 shows the N_2 adsorption−desorption isotherm and the pore size distribution of the Ag−hollandite nanofibers synthesized at 160 °C with a 2/3 $AgMnO_4/Mn(NO_3)_2$ molar ratio. The isotherm corresponded to Type II adsorption with a steep increase at low p/p_0 and capillary condensation at high p/p_0, indicating the presence of micropores and slit-shaped capillaries with parallel plates. The Ag−hollandite nanofibers exhibited one narrow pore size distribution in the micropore range with a pore diameter around 0.5 nm, close to the tunnel size of 0.46 nm. This result indicates that the microporous structure of the Ag−hollandite nanofibers is similar to those of the K−OMS-2 materials.[8,15]

Formation Mechanism of the Ag−Hollandite Nanofibers. To elaborate the growing mechanism of the Ag−hollandite nanofibers, we examined the samples at different

(14) (a) Wang, Z. M.; Tezuka, S.; Kanoh, H. *Chem. Mater.* 2001, 13, 530−537. (b) O'Young, C. L.; Sawicki, R. A.; Suib, S. L. *Microporous Mater.* **1997**, *11*, 1−8.
(15) Villegas, J. C.; Garces, L. J.; Gomez, S.; Durand, J. P.; Suib, S. L. *Chem. Mater.* **2005**, *17*, 1910−1918.

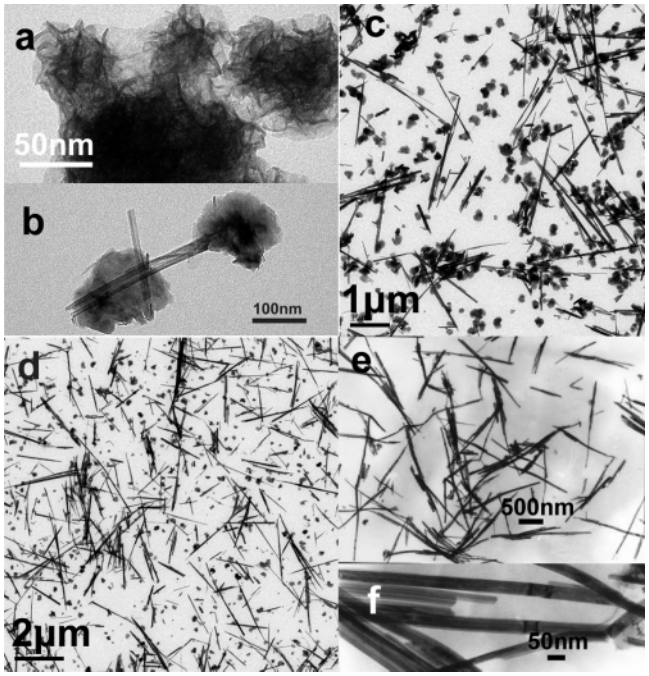

Figure 5. TEM images of the samples at different stages of hydrothermal synthesis: (a) precursor at room temperature, and at 160 °C for (b) 0.5, (c) 1, (d) 6, and (e, f) 12 h.

stages during the hydrothermal synthesis at 160 °C by XRD measurements and TEM observations, as shown in Figures 4 and 5. For the sample obtained by mixing $AgMnO_4$ and $Mn(NO_3)_2$ (molar ratio of 2/3) aqueous solutions at room temperature, the precursor was amorphous with lamellar morphology. When the hydrothermal synthesis was conducted for 0.5 h, the sample was still amorphous. But the TEM image showed that the lamellar structures begun to curl and that some tubular structures appeared. When the synthesis time was prolonged to 1 h, the sample showed similar diffractions to Ag−hollandite but with poor crystallinity. TEM images further indicated that nanorods and nanofibers were formed with the coexistence of lamellar particles. A significant increase in the crystallinity was observed for the sample synthesized for 6 h, evidenced by the relative intensive diffraction peaks. Meanwhile, the TEM image showed that many more and much longer nanofibers were forming and that the lamellar particles were decreasing. When the hydrothermal synthesis was conducted for 12 h, highly crystallized Ag−hollandite nanofibers were obtained and there were no lamellar particles any more. Therefore, it is possible to assume the growing mechanism of Ag−hollandite nanofibers as follows. Lamellar MnOx species were initially formed by mixing $AgMnO_4$ and $Mn(NO_3)_2$ aqueous solutions at room temperature. Under hydrothermal conditions, the MnOx layer begun to curl into a tubular structure. Because of the presence of Ag^+, the lamellar structure of MnOx could further transfer into a tunnel structure of Ag−hollandite. When the synthesis period was prolonged, the tubular and curling lamellar structures gradually grew into nanofibers and the lamellar particles decreased and finally disappeared. This phenomenon is similar to the formation of nanorods from lamella.[13]

Figure 6 further shows the HRTEM images of the Ag−hollandite nanofibers synthesized at 160 °C for 12 h. The FTT pattern indicated that the view direction was.[010] The fringe spacings of 0.49 and 0.27 nm represented the lattice spacings of the (200) and (101) planes, respectively, in the crystal structure of Ag−hollandite. The crystalline growth of the Ag−hollandite nanofibers was along the [001] direction, and the predominantly exposed planes were (200) and (101).

XPS Surface Analysis. Figure 7a displays the XP spectra of Mn 2p in the Ag−hollandite nanofibers. The binding energies of Mn $2p_{3/2}$ and Mn $2p_{1/2}$ were 642.2 and 653.9 eV, respectively, which can be attributed to a mixture of $Mn^{4+}$and Mn^{3+} species.[16] Because Mn^{2+}, Mn^{3+}, and Mn^{4+} have essentially the same binding energy in the perovsksite sample,[17] it is difficult to identify the oxidation state of manganese by only the binding energy shift of Mn 2p. Detailed studies by Galakhov et al.[18] revealed that the XPS of Mn 3s is more promising for identifying manganese oxidation state, and the magnitude of the Mn 3s splitting decreased monotonously with increasing the average oxidation state (AOS) of manganese. Figure 7b shows the XPS of Mn 3s in the Ag−hollandite nanofibers. The binding energy difference (ΔE_{3s}) between the main peak and its satellite was 4.5 eV, from which the AOS of manganese was evaluated to be 3.9. That is, Mn^{4+} was dominantly presented in the Ag−hollandite nanofibers.

Figure 7c shows the core-level XP spectra of Ag 3d in the Ag-hollandite nanofibers. The Ag $3d_{5/2}$ and Ag $3d_{3/2}$ peaks were centered at 367.8 and 373.8 eV, respectively, characteristics of Ag^+ species.[19] Figure 7d further shows the Ag MVV spectra. The Auger parameter (α'), which is defined as the sum of the kinetic energy of the Auger electron (Ag M_4VV) and the binding energy of the core level (Ag $3d_{5/2}$),[19b,20] was calculated to be 724.7 eV. Because the Auger parameters for Ag and Ag_2O were 726.1 and 724.4 eV,[20] respectively, the silver species in the Ag−hollandite nanofibers can be assumed to be Ag^+.

Thermal Stability. Figure 8 shows the TG plot and the temperature-programmed decomposition profile of the Ag−hollandite nanofibers. The weight loss could be categorized into four segments. The initial weight loss of 5.0% below 360 °C with two peaks appearing at 116 and 270 °C was due to the removal of physically and chemically adsorbed water (2.4 and 2.6%, respectively), in good agreement with previous observations.[2a,4b,7a] The following three weight losses in the temperature range of 360−780 °C corresponded to the release of oxygen. The first oxygen loss (4.4%)

(16) (a) Ge, J. H.; Zhou, L. H.; Yang, F.; Tang, B.; Wu, L. Z.; Tung, C. H. *J. Phys. Chem. B* **2006**, *110*, 17854−17859. (b) Tjeng, L. H.; Meinders, M. B. J.; Van, Elp, J.; Ghijsen, J.; Sawatzsky, G.; Johnson, R. L. *Phys. Rev. B* **1990**, *41*, 3190−3199.
(17) Castro, V. D.; Polzonetti. G.; *J. Electron Spectrosc. Relat. Phenom.* 1989, 48, 117−123.
(18) Galakhov, V. R.; Demeter, M.; Bartkowski, S.; Neumann, M.; Ovechkina, N. A.; Kurmaev, E. Z.; Lobachevskaya, Y. M.; Mitchell, J.; Ederer, D. L. *Phys. Rev. B* **2002**, *65*, 113102.
(19) (a) Gao, X. Y.; Wang, S. Y.; Li, J.; Zheng, Y. X.; Zhang, R. J.; Zhou, P.; Yang, M. Y.; Chen, L. Y. *Thin Solid Films* 2004, 455−456, 438−442. (b) Tjeng, L. H.; Meinders, M. B. J.; Vanelp, J.; Ghijsen, J.; Sawatzky, G. A.; Johnson, R. L. *Phys. Rev. B* **1990**, *41*, 3190−3199.
(20) (a) Scheon, G. *Acta Chem. Scand.* **1973**, *27*, 2623−2633. (b) Wagner, C. D. *Discuss. Faraday Soc.* **1975**, *60*, 291−300.

Table 1. Textural Properties of the Ag−Hollandite Nanofibers

		surface area (m^2/g)			pore volume (cm^3/g)	
$AgMnO_4/Mn(NO_3)_2$ ratio	Ag/Mn ratio[a]	S_{mic}[b]	S_{ext}[c]	S_{BET}	V_{mic}[b]	V_{total}
5/2	0.111	5.7	40.5	46.1	0.00144	0.395
2/3	0.087	6.7	35.6	42.4	0.00237	0.373

[a] ICP analysis. [b] Micropores. [c] External surface.

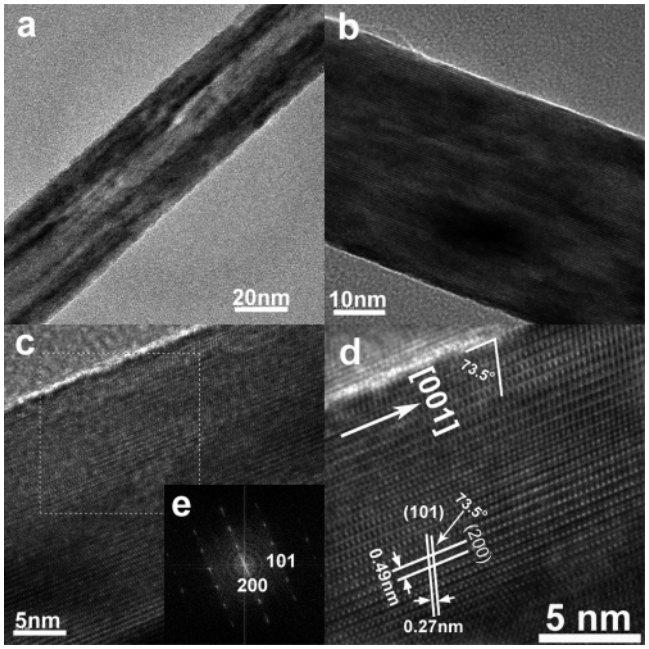

Figure 6. HRTEM images of the Ag−hollandite nanofibers.

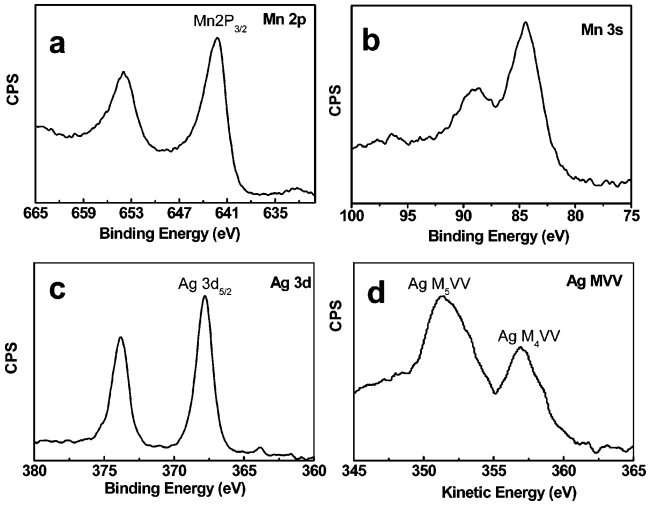

Figure 7. XP spectra of Mn 2p, Mn 3s, Ag 3d, and Ag MVV in the Ag−hollandite nanofibers.

occurred at 360−530 °C, the second evolution (4.3%) took place at 530−630 °C, and the third (1.9%) occurred at 630−780 °C.

Oxygen release from hollandite-type manganese oxides usually leads to the formation of oxygen deficient products such as bixbyite (Mn_2O_3) and hausmannite (Mn_3O_4), and consequently, would cause the collapse of the tunnel at high temperatures.[2a,21] For the Ag−hollandite nanofibers, the chemical composition was formulated as $Ag_{0.7}Mn_8O_{16}\cdot 2.3H_2O$ on the basis of the elemental analysis and the amount of H_2O from the TG measurement. Theoretically, the weight losses of the Ag−hollandite nanofibers are subject to three predominant steps

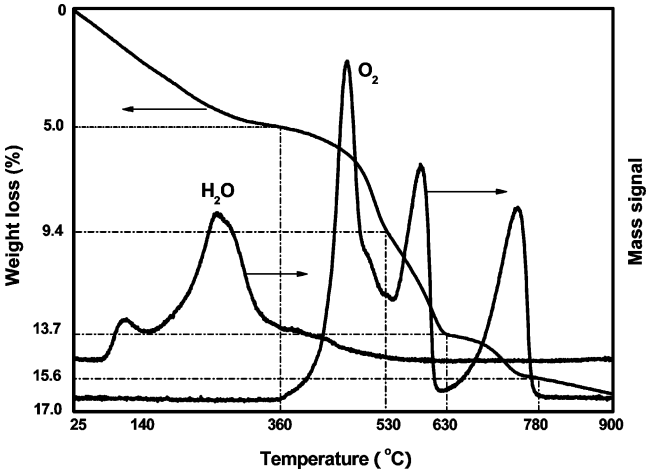

Figure 8. TGA plot and temperature-programmed decomposition MS profile of the Ag−hollandite nanofibers.

$$Ag_{0.7}Mn_8O_{16}\cdot 2.3H_2O \xrightarrow[-H_2O]{-5.0\%} Ag_{0.7}Mn_8O_{16} \xrightarrow[-[O]]{-7.9\%}$$
$$0.7Ag + Mn_2O_3 \xrightarrow[-[O]]{-2.7\%} 0.7Ag + 8/3Mn_3O_4$$

The initial weight loss of 5.0% is due to water desorption, and the following oxygen evolution includes two steps: the first step occurs at relatively lower temperature with a weight loss of 7.9% and the Ag−hollandite nanofibers are simultaneously transformed into Mn_2O_3 and Ag; the second step takes place at higher temperature with a weight loss of 2.7% and the Mn_2O_3 species is further converted into Mn_3O_4 spinel. Theoretically, the total weight loss for the Ag−hollandite nanofibers with chemical composition of $Ag_{0.7}Mn_8O_{16}\cdot 2.3H_2O$ to Mn_3O_4 and Ag should be 15.6%.

Accordingly, the weight loss (4.4%) at 360−530 °C in Figure 8 could be attributed to the evolution of oxygen bridging Ag and Mn, and the Mn species adjacent to the bridging oxygen was simultaneously transformed into Mn_2O_3. The next peak of oxygen evolution (4.3%) at 530−630 °C originated from the combined oxygen release of Ag_2O to Ag and MnO_2 away from silver species to Mn_2O_3. The total weight loss of oxygen at this stage is 8.7%, which is larger than the theoretical value of 7.9%, suggesting that a small fraction of Mn_2O_3 in the vicinity of silver species was already transformed into Mn_3O_4 spinel. This phenomenon could be attributed to the possible oxygen spillover from MnOx octahedra to Ag^+ through the Ag−O−Mn bridge. Imamura et al.[22a] found that the lattice oxygen belonging to Ag in the Ag/MnO_x composite could be easily liberated upon heating under an inert atmosphere, but Ag could still maintain its

(21) Tanaka, Y.; Tsuji, M.; Tamaura, Y. *Phys. Chem. Chem. Phys.* **2000**, *2*, 1473−1479.

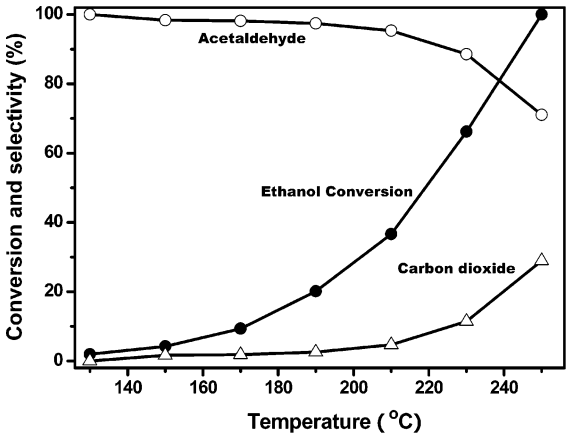

Figure 9. Conversion of ethanol and selectivities of acetaldehyde and carbon dioxide over the Ag−hollandite nanofibers as a function of reaction temperature. Feed stream, 5%C_2H_5OH/10%O_2/He; GHSV, 36 000 mL g^{-1} h^{-1}. ●, Ethanol conversion; ○, acetaldehyde selectivity; and □, selectivity of CO_2.

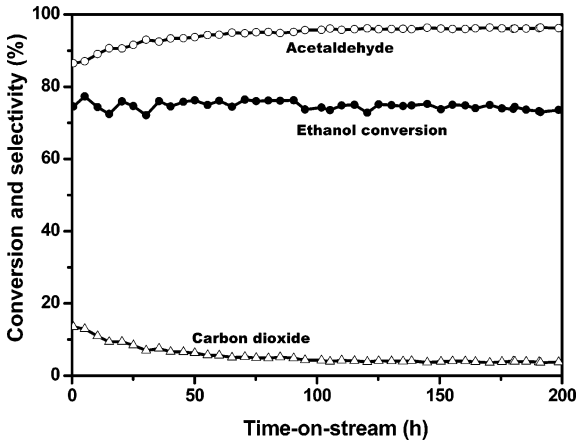

Figure 10. Stability test of the Ag−hollandite nanofibers for ethanol oxidation at 230 °C. Feed stream, 5%C_2H_5OH/10%O_2/He; GHSV, 36 000 mL g^{-1} h^{-1}. ●, Ethanol conversion; ○, acetaldehyde selectivity; and □, selectivity of CO_2.

oxidation state because of oxygen spillover from MnO_x. Watanabe et al.[22b] and our recent work[22c] of Ag/MnO_x composites also demonstrated that manganese oxide could supply oxygen to silver, keeping silver in oxidative state. The last oxygen evolution at 630−780 °C could be assigned to the decomposition of the residual Mn_2O_3 to Mn_3O_4 spinel. The weight loss (1.9%) was less than the theoretical value of 2.7%. However, the total weight loss of oxygen was still 10.6%, exactly equal to the theoretical value for the transformation of $Ag_{0.7}Mn_8O_{16}$ to Mn_3O_4 and Ag.

Catalytic Performance for Ethanol Oxidation. Catalytic oxidation of ethanol is one of the commercial processes for producing acetaldehyde using silver as catalyst. The reaction is generally operated at 480 °C with ethanol conversion of 74−82% and acetaldehyde selectivity of no more than 80%.[23] Zhou et al.[24] investigated the catalytic performance of manganese oxide octahedral molecular sieves with the doping of Ni^{2+}, Cu^{2+}, Fe^{3+}, Co^{2+}, and Zn^{2+} and found that the conversion of ethanol and the selectivity of acetaldehyde were strongly dependent on the transition metal dopants in the OMS-2 framework. Particularly, the Fe−OMS-2 catalyst showed the highest ethanol conversion of 71.5% and acetaldehyde selectivity of 78.9% selectivity at 300 °C.

The catalytic reactivity of the Ag−hollandite nanofibers was evaluated for ethanol oxidation. Acetaldehyde and carbon dioxide were detected to be the only products. Figure 9 shows the conversion of ethanol and the selectivities of acetaldehyde and CO_2 over the Ag−hollandite nanofibers as a function of reaction temperature. The conversion of ethanol increased rapidly with temperature and reached 100% at 250 °C. The selectivity of acetaldehyde was almost 100% below 170 °C, indicating that ethanol was exclusively converted into acetaldehyde. Further increase in the reaction temperature resulted in significant decrease in the selectivity of acetaldehyde due to the formation carbon dioxide. Accordingly, the yield of acetaldehyde increased monotonously with increasing the conversion of ethanol, and reached a maximum of 71% when total conversion of ethanol was achieved at 250 °C. Figure 10 shows the conversion of ethanol and the selectivities of acetaldehyde and CO_2 over the Ag−hollandite nanofibers as a function of time-on-stream at 230 °C. During the initial 50 h, the selectivity of acetaldehyde was gradually increased from 86 to 95%, whereas the selectivity of CO_2 was deceased from 14 to 5%. Thereafter, the conversion of ethanol was about 75% and the selectivity of acetaldehyde maintained at about 95%. This result clearly demonstrated that the Ag−hollandite nanofibers could show rather high stability for ethanol oxidation in addition to its high ethanol conversion and acetaldehyde selectivity.

Xia et al.[5] pointed out that the Ag−O−Mn bridge in Ag−hollandite could facilitate the electron transfer between Ag and Mn through the bridged oxygen, which was more mobile and active. Shen et al.[11b] also attributed the quite high activity and selectivity of nanosilver/zeolite film/copper grid catalysts for gas-phase oxidation of alcohols to the stable presence of large amount of Ag^+ species and $Ag_n^{\delta+}$ clusters. Thus, it is highly probable that the Ag^+ species in the Ag−hollandite nanofibers facilitated the activation of molecular oxygen and its transfer to oxidize ethanol through the Ag−O−Mn bridge. Meanwhile, the unique crystal structure as well as the morphology of the Ag−hollandite nanofibers may be responsible for the rather high catalytic stability in ethanol oxidation.

Conclusions

The temperature significantly affected both the crystal structure and the morphology of the Ag−hollandite nanofibers. The concentration of Ag^+ in the range of 0.025−0.056 mol/L did not influence the crystal structure, but significantly affected the morphology of Ag−hollandite nanofibers. Very uniform Ag−hollandite nanofibers with diameters of 20−40 nm and lengths of 0.5−4 μm was prepared by hydrothermal synthesis at 160 °C and a 2/3 $AgMnO_4$/$Mn(NO_3)_2$

(22) (a) Imamura, S. *Ind. Eng. Chem. Res.* **1999**, *38*, 1743−1753. (b) Watanabe, N.; Yamashita, H.; Miyadera, H.; Tominaga, S. *Appl. Catal., B* **1996**, *8*, 405−415. (c) Tang, X. F.; Chen, J. L.; Li, Y. G.; Li, Y.; Xu, Y. D.; Shen, W. J. *Chem. Eng. J.* **2006**, *118*, 119−125.
(23) Faith, W. L.; Keyes, D. B.; Clark, R. L. *Industrial Chemicals*, 2nd ed.; Wiley: New York, 1957; pp 2−3.
(24) Zhou, H.; Wang, J. Y.; Chen, X.; O'Young, C. L.; Suib, S. L. *Microporous Mesoporous Mater.* **1998**, *21*, 315−324.

molar ratio. Silver presented as Ag^+ and the average oxidation state of manganese was 3.9 in the Ag−hollandite nanofibers. Under hydrothermal condition, the initially formed lamellar MnOx species could curl into tubular structure with the presence of Ag^+ and gradually transferred into the tunnel structure of Ag−hollandite nanofibers. When used for ethanol oxidation, the conversion of ethanol reached 100% at a temperature as low as 250 °C with acetaldehyde selectivity of 71%. In addition to this extremely high activity and selectivity, the Ag−hollandite nanofibers showed rather high stability with ethanol conversion of 75% and acetaldehyde selectivity of 95% at 230 °C for 200 h time-on-stream operation. The stable presence of Ag^+ and the unique morphology of the Ag−hollandite nanofibers were supposed to play critical roles in determining the high catalytic activity and stability for ethanol oxidation.

CM070904K